Ferromagnetic resonance investigation of magnetic anisotropy in $Ga_{1-x}Mn_xAs$ synthesized by ion implantation and pulsed laser melting

Y. Y. Zhou, X. Liu,[*] and J. K. Furdyna[†]

Department of Physics, University of Notre Dame, Notre Dame, Indiana 46556, USA

M. A. Scarpulla and O. D. Dubon

Department of Materials Science and Engineering, University of California at Berkeley, Berkeley, California 94720, USA

A systematic investigation of ferromagnetic resonance (FMR) was carried out on $Ga_{1-x}Mn_xAs$ layers synthesized by Mn ion implantation into GaAs followed by pulsed laser melting. Angular and temperature dependences of FMR were measured on layers prepared on GaAs (001), (110), and (311) surfaces. The observed angular dependence of FMR can be understood in terms of contributions from cubic anisotropy fields defined by the crystal symmetry of $Ga_{1-x}Mn_xAs$ and uniaxial anisotropy fields perpendicular or parallel to the film plane. For completeness, the angular dependence of the FMR linewidth was also investigated and was found to be dominated by broadening ascribed to local inhomogeneities in magnetic anisotropy. Our results show that both the magnetic anisotropy and the FMR linewidth in (Ga,Mn)As prepared by ion implantation are similar to those observed on $Ga_{1-x}Mn_xAs$ samples grown by low-temperature molecular beam epitaxy, indicating that the two very different growth methods lead to materials with fundamentally similar magnetic properties.

PACS number(s): 75.50.Pp, 76.50.+g, 61.72.U−, 75.70.Ak

I. INTRODUCTION

The ferromagnetic semiconductor $Ga_{1-x}Mn_xAs$ has been the subject of extensive studies both because of its fundamental physical properties (many of which are still not fully understood) and because of the prospects which it offers for applications in spin electronics.[1,2] The vast majority of research on this material was carried out on $Ga_{1-x}Mn_xAs$ grown by low-temperature molecular beam epitaxy (LT-MBE), low-temperature growth being necessary to circumvent the very low solubility limits of Mn in the GaAs host.[3] Recently an alternative way of fabricating high-quality ferromagnetic $Ga_{1-x}Mn_xAs$ has been discovered, using ion implantation (II) of Mn into GaAs followed by pulsed laser melting (PLM), a rapid liquid-phase epitaxial growth process that recrystallizes the ion-damaged film.[4,5] The differences between the LT-MBE and the II-PLM are expected to result in some differences between materials prepared by the two methods, perhaps the most notable being that the LT-MBE growth leads to the formation of Mn interstitials while $Ga_{1-x}Mn_xAs$ prepared by II-PLM has been shown to be interstitial free.[6] However, the electrical and magnetic properties of films grown via the two methods have been shown to be nearly identical.[6] Since magnetic anisotropy plays a key function in determining the magnetic properties of $Ga_{1-x}Mn_xAs$ and is also expected to play a major role in designing $Ga_{1-x}Mn_xAs$-based devices, it is especially important to obtain a thorough understanding of magnetic anisotropy in II-PLM $Ga_{1-x}Mn_xAs$ and how this property differs (if at all) from magnetic anisotropy of $Ga_{1-x}Mn_xAs$ grown by LT-MBE.

Ferromagnetic resonance (FMR) is a powerful technique for studying magnetic anisotropy in thin ferromagnetic layers.[7,8] In the present paper we use this technique to investigate magnetic anisotropy parameters in $Ga_{1-x}Mn_xAs$ samples synthesized by II-PLM, which can then be com-

pared to the properties of magnetic anisotropy observed on $Ga_{1-x}Mn_xAs$ grown by LT-MBE. The information on magnetic anisotropy can be obtained directly by studying the dependence of FMR on the direction of applied magnetic field with respect to the crystal axes, typically carried out by rotating the field in some crystal plane. Earliest studies of FMR in $Ga_{1-x}Mn_xAs$ were performed on $Ga_{1-x}Mn_xAs$ fabricated by LT-MBE using films grown on (001) planes, which automatically limits the selection of geometries in which the angular dependence of FMR can be studied. Furthermore, LT-MBE $Ga_{1-x}Mn_xAs$ simply does not grow well on certain planes, such as the (110) plane. $Ga_{1-x}Mn_xAs$ samples fabricated by II-PLM offer a special advantage in this respect since fabrication of $Ga_{1-x}Mn_xAs$ layers by the latter method on higher-index planes [e.g., (110), (311)] may be carried out with fewer added difficulties, thus offering a number of options for mapping out the properties of magnetic anisotropy in this material. In the present paper we make use of this feature by carrying out FMR measurements as a function of angle in certain higher-index crystallographic planes which had not been explored in earlier studies. Thus, in addition to providing valuable information on the symmetry of magnetic anisotropy generally, these studies also serve to illustrate the behavior of FMR in hitherto unexplored geometries.

This paper is organized as follows. In Sec. II we describe the sample preparation and FMR experimental details. Section III discusses the theoretical model used to analyze the dependence of the FMR field on the orientation of the applied magnetic field, with special emphasis on the effects of magnetic anisotropy. The observed angular dependence of the resonance field in various crystallographic planes is presented and discussed in Sec. IV. This serves to obtain magnetic anisotropy parameters for the II-PLM samples studied in this paper. For completeness, in Sec. V we discuss the behavior of FMR linewidth and its dependence on magnetic anisotropy. Although the linewidth results are discussed in

empirical terms, they are sufficient to establish that in $Ga_{1-x}Mn_xAs$ samples synthesized by II-PLM, as in the earlier studies of $Ga_{1-x}Mn_xAs$ grown by LT-MBE, the resonance linewidth is governed primarily by local magnetic inhomogeneities.

II. SAMPLE PREPARATION AND EXPERIMENTAL DETAILS

A. Film growth by ion implantation and pulsed laser melting

$Ga_{1-x}Mn_xAs$ specimens used in this study were prepared by implantation of Mn ions into a GaAs substrate followed by PLM. In ion implantation (II), Mn ions are accelerated by an electric potential to energies typically in the range of 10 to 1000 keV and are directed onto the GaAs substrate at typical doses of 10^{14}–10^{16} ions/cm^2. The ion implantation results in an approximately Gaussian depth profile of Mn concentration within the GaAs substrate that can be characterized by its width and the location of its center, both of which scale with incident energy.

When the implanted ions come to rest, they may or may not inhabit substitutional Ga lattice sites and post-implantation annealing of some form is then necessary to allow them to diffuse onto those sites. Pulsed laser melting is a highly effective method for converting the disordered implanted region into thin layers of crystalline ferromagnetic III-Mn-V alloys. As an example, a single pulse (~30 ns) from a KrF excimer laser ($\lambda = 248$ nm, $E_{photon} = 5$ eV, fluence 0.2–0.5 J/cm^2), after being spatially homogenized, is directed onto an implanted substrate. The absorption length for the UV photons in amorphous GaAs is approximately 15 nm. Thus most of the laser energy is restricted to the near surface region and converted to heat. As the heat flows into the substrate, the liquid/solid interface moves through the ion-damaged region into the underlying substrate, which seeds single-crystalline epitaxial solidification as the liquid/solid front returns to the surface. The short times and small distances typical for this process result in truly unparalleled solidification characteristics, involving solidification velocities of a few m/s and cooling rates of 10^9–10^{10} K/s. Such high velocities result in a departure from local equilibrium at the interface referred to as solute trapping,[9] whereby the implanted atoms are essentially buried in the growing crystal at concentrations far in excess of the equilibrium solubility limits, because the solidification rate exceeds the diffusive velocity. In the case of Mn in GaAs the equilibrium solubility limit appears to be in the range of 10^{18}–10^{19} cm^{-3}, while the II-PLM process routinely produces films with Mn concentrations in the range of 10^{21} cm^{-3}.

The experiments described in this paper involve a series of $Ga_{1-x}Mn_xAs$ layers synthesized by the II-PLM method on the following GaAs surface planes: (001), (110), (311)A, and (311)B. To allow meaningful comparison between measurements on samples with different orientations, all samples were grown using the same Mn ion dosage (1.5 $\times 10^{16}$ Mn ions/cm^2), Mn ion energy (50 keV), and the same KrF excimer laser fluence (0.30 J/cm^2). These conditions are identical to those used by Scarpulla *et al.*[6] in preparing their sample A, which showed a Curie temperature of
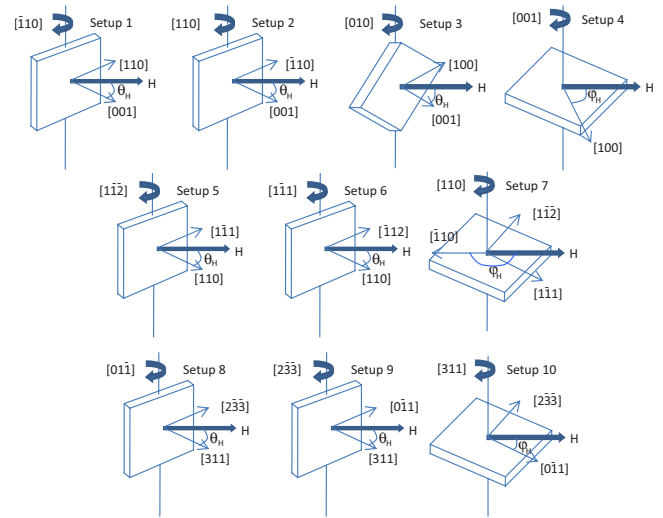

FIG. 1. (Color online) Four experimental configurations used in the present study. For the (001) sample (sample A) the orientation of the dc magnetic field **H** can be varied in the ($\bar{1}10$), (110), (010), and (001) planes (setups 1, 2, 3, and 4); for the (110) sample (sample B) the orientation of **H** can be varied in the ($1\bar{1}2$), ($1\bar{1}1$), and (110) planes (setups 5, 6, and 7); and for the (311) sample [sample C] the **H** orientation can be varied in the ($0\bar{1}1$), ($2\bar{3}3$), and (311) planes (setups 8, 9, and 10). Crystal orientations for the (311)B sample (sample D) are as for setups 8, 9, and 10, but with Miller index signs in the horizontal plane reversed.

~100 K (see Table I in that reference) and an estimated concentration of substitutional Mn of ca. 4.0%. Although there can be differences in Mn distributions for different substrate orientations, under identical conditions of II-PLM synthesis these differences are expected to be small, and we will therefore assume that the Mn concentration in the sample series used in this study is also ~4.0%. In what follows we will refer to the layers with the (100), (110), (311)A, and (311)B orientations as samples A, B, C, and D, respectively.

B. Experimental details of FMR measurements

The FMR measurements were carried out at 9.4 GHz (*X* band) using a Bruker electron paramagnetic resonance (EPR) spectrometer. Note that the dc magnetic field of the EPR spectrometer is confined to the horizontal plane and the microwave (rf) field is vertical. The magnetic film is placed in a suprasil sample tube connected to a liquid helium continuous flow cryostat. The sample-containing tube is then inserted into the microwave cavity of the EPR spectrometer. The helium flow is driven by a small-diaphragm vacuum pump which circulates the cold helium gas through the tube. The underpressure produced by the pump is sufficient to achieve temperatures down to 3.6 K and a heater along the helium path provides a means of controlling the sample temperature. The angular dependence of FMR is obtained by rotating the sample tube.

The (001), (110), and (311) $Ga_{1-x}Mn_xAs$ layers are cleaved into rectangular pieces, which are then placed in the sample tube in specific orientations, as shown in Fig. 1. We

first consider the experimental configurations for the (001) samples in some detail. Setup 1 in Fig. 1 represents the geometry where the sample plane and the $[\bar{1}10]$ edge are both vertical, allowing angular FMR measurements in the $(\bar{1}10)$ plane, from **H**∥[001] (normal field orientation) to the in-plane **H**∥[110] orientation. In setup 2 the sample plane and the [110] direction are also vertical, allowing FMR measurements in the (110) plane from the **H**∥[001] (normal orientation) to the in-plane **H**∥[$\bar{1}10$] configuration. In setup 3 the sample is mounted with the [010] direction in the plane of the film vertical, which allows angular FMR measurements in the (010) plane, between the normal **H**∥[001] and the in-plane **H**∥[100] orientations. In setup 4 the sample plane is horizontal, allowing us to map out the angular FMR behavior when **H** is confined to the layer [i.e., to the (001)] plane. Similarly, for the (110) sample we measure FMR in setups 5–7, with fields and crystallographic orientations shown in Fig. 1. Finally, for the (311)A samples the geometries of the FMR measurements are shown as setups 8–10. Geometries for the (311)B sample can be obtained simply by changing the signs of the Miller indices in the plane of rotation shown for the (311)A case in Fig. 1.

III. THEORETICAL MODEL FOR FMR IN THIN GAMNAS LAYERS

The theoretical formulation of FMR is based on the Landau-Lifshitz-Gilbert (LLG) equation, which describes both the precession of magnetization and its damping,[10,11]

$$-\frac{1}{\gamma}\frac{\partial \mathbf{M}}{\partial t} = \mathbf{M} \times \left(-\frac{\partial F}{\partial \mathbf{M}} + \mathbf{h}\right) - \frac{\alpha}{(\gamma \cdot M_S)} \cdot \left[\mathbf{M} \times \frac{\partial \mathbf{M}}{\partial t}\right].$$

(1)

Here $\gamma = g\frac{\mu_B}{\hbar}$ and $\alpha = \frac{G}{\gamma \cdot M_S}$ are the gyromagnetic ratio and the damping coefficient, respectively; G and M_S are the Gilbert coefficient and the saturation magnetization; **M**, F, and **h** denote magnetization, magnetic-free-energy density, and the microwave magnetic field, respectively; and g, μ_B, and $\hbar$ have their standard meaning. For the purpose of determining the position of FMR we will only need to use the first term of Eq. (1); and we will return to the second (damping) term in Sec. V, when we discuss the resonance linewidth.

Our main objective in this paper is to determine the magnetic anisotropy parameters for II-PLM $Ga_{1-x}Mn_xAs$. Expressing Eq. (1) in terms of F is particularly convenient for
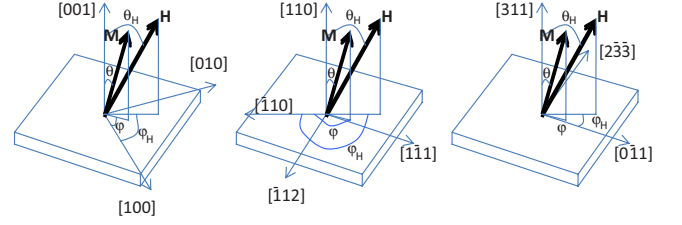

FIG. 2. (Color online) Coordinate systems used in this paper. The orientation of the dc applied magnetic field **H** is described by θ_H, φ_H. The resulting equilibrium orientation of the magnetization **M** is given by (θ, φ). From left to right: the (001) sample (sample A); the (110) sample (sample B); and the (311)A sample (sample C).

this purpose since F can be expressed in terms of magnetic anisotropy fields as a function of orientation of the applied magnetic field for various sample geometries used in this study.[12] The resulting FMR fields as a function of field orientation can then be used to fit the observed angular dependence of FMR, using the anisotropy fields as fitting parameters.

For samples formed on (001) GaAs surfaces the free energy density F has the following form:[7,13]

$$F_{001} = -MH[\cos \theta \cos \theta_H + \sin \theta \sin \theta_H \cos(\varphi - \varphi_H)]$$

$$+ 2\pi M^2 \cos^2 \theta - \frac{1}{2}MH_{2\perp} \cos^2 \theta$$

$$-\frac{1}{2}MH_{2\parallel} \sin^2 \theta \sin^2\left(\varphi - \frac{\pi}{4}\right) - \frac{1}{4}MH_{4\perp} \cos^4 \theta$$

$$-\frac{1}{4}MH_{4\parallel}\frac{1}{4}(3 + \cos 4\varphi)\sin^4 \theta.$$

(2)

Here the first term describes the Zeeman energy; the second term represents demagnetizing energy (sometimes referred to as shape anisotropy); the angles θ, φ, θ_H, and φ_H are defined in Fig. 2 for all samples; $H_{2\perp}$ and $H_{4\perp}$ are uniaxial and cubic anisotropy fields perpendicular to the sample plane, respectively; and $H_{2\parallel}$ and $H_{4\parallel}$ are, respectively, uniaxial and cubic anisotropy fields in the sample plane. For simplicity in calculation, in what follows we will lump the $4\pi M - H_{2\perp}$ together into a single term defined as H_{eff}.

Similarly, by using direction cosines appropriate for the crystallographic plane (110), we obtain the free energy density F_{110} for the (110) sample (sample B) in the form:[14]

$$F_{110} = -MH[\cos \theta \cos \theta_H + \sin \theta \sin \theta_H \cos(\varphi - \varphi_H)] + \frac{1}{2}MH_{eff}\cos^2 \theta - \frac{1}{4}MH_{4\perp}\left(-\frac{1}{\sqrt{2}}\sin \theta \cos \varphi + \frac{1}{\sqrt{2}}\cos \theta\right)^4$$

$$-\frac{1}{4}MH_{4\parallel}\left[\left(\frac{1}{\sqrt{2}}\sin \theta \cos \varphi + \frac{1}{\sqrt{2}}\cos \theta\right)^4 + (\sin \theta \sin \varphi)^4\right],$$

(3)

where the angles θ, φ, θ_H, and φ_H are now measured with respect to the axes shown in the central part of Fig. 2. Finally, using direction cosines appropriate for the (311) crystallographic plane we obtain the free energy density F_{311} for samples grown on (311) GaAs surfaces:[12,14]

$$F_{311} = -MH\left[\cos\theta\cos\theta_H + \sin\theta\sin\theta_H\cos(\varphi-\varphi_H)\right] + \frac{1}{2}MH_{eff}\cos^2\theta - \frac{1}{4}MH_{4\perp}\left(-\sqrt{\frac{2}{11}}\sin\theta\cos\varphi + \frac{3}{\sqrt{11}}\cos\theta\right)^4$$

$$-\frac{1}{4}MH_{4\|}\left[\left(\frac{3}{\sqrt{22}}\sin\theta\cos\varphi - \frac{1}{\sqrt{2}}\sin\theta\sin\varphi + \frac{1}{\sqrt{11}}\cos\theta\right)^4 + \left(\frac{3}{\sqrt{22}}\sin\theta\cos\varphi + \frac{1}{\sqrt{2}}\sin\theta\sin\varphi + \frac{1}{\sqrt{11}}\cos\theta\right)^4\right]. \quad (4)$$

Note that in Eqs. (3) and (4) we no longer use $H_{2\|}$. This is because that term arises from the (still not fully understood) magnetic anisotropy associated with differences between the [110] and the [1$\bar{1}$0] directions. The $H_{2\|}$ parameter is simple to identify in analyzing the FMR results obtained on samples grown on the (001) plane.[15] However, for layers formed on other surfaces the situation is more complex. In the case of the (110) plane it is readily seen that all effects arising from the small differences between the [110] and the [1$\bar{1}$0] directions will be overwhelmed by the large effect of H_{eff} normal to that plane. And in the case of the (311) samples, it is very difficult to distinguish between the effects of [110] and [1$\bar{1}$0]. Since (as will be seen below) the $H_{2\|}$ is very small compared to other anisotropy parameters, we will simplify the analysis by assuming its contribution to Eqs. (3) and (4) to be negligible.

It should also be noted that in the case of samples grown on (001) GaAs substrates the axes of cubic (i.e., $H_{4\|}$ and $H_{4\perp}$) and uniaxial (i.e., $H_{2\|}$ and H_{eff}) anisotropies coincide with the axes of the crystal coordinate system (and thus also with each other). However, in the case of the (110) and (311) GaAs samples, the axes of cubic and uniaxial anisotropy no longer coincide. In general the effective anisotropy term H_{eff} is always along the direction normal to the sample surface while the cubic anisotropy is always defined along the crystallographic axes $\langle 100 \rangle$.

IV. OBSERVED BEHAVIOR OF FMR FIELDS AND DISCUSSION

Our emphasis in this section will be on the dependence of the FMR field on the direction of applied magnetic field, from which we will obtain the anisotropy parameters for II-
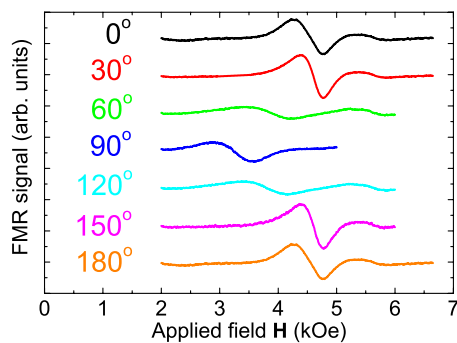
FIG. 3. (Color online) Selected FMR spectra for sample A taken at 4 K from $\theta_H=0°$ to 180°, with **H** in the ($\bar{1}$10) plane (setup 1).

PLM Ga$_{1-x}$Mn$_x$As samples. Then, by measuring the angular dependence of FMR at a series of temperatures, we will also be able to obtain the dependence of magnetic anisotropy parameters on temperature. As already noted, in discussing the data we will refer to samples synthesized on (001), (110), (311)A, and (311)B as sample A, B, C, and D, respectively.

A. Results for II-PLM GaMnAs formed on the (001) plane

To obtain the angular dependence of FMR for the Ga$_{1-x}$Mn$_x$As sample grown on the (001) plane (sample A), we measured the resonance spectra as a function of magnetic field orientation taken in 6° steps over a 180° range in each of the setups 1 through 4 shown in Fig. 1. As an example of raw data, Fig. 3 shows the FMR spectra observed at 4 K on sample A for a series of field orientations in setup 1, i.e., for magnetic field **H** rotated in the ($\bar{1}$10) plane. The position of the resonance is symmetric about the 90° orientation of setup 1 as expected for the cubic geometry. The cause of the much weaker resonances seen at fields above FMR in the near-normal field orientations (i.e., near 0° and 180°) is unclear although it could be related to departures from the Gaussian depth profile of the Mn concentration within the samples.

Figure 4(a) shows the angular dependence of the FMR position for sample A measured at 4 K for setups 1, 2, and 3, corresponding to the applied field **H** rotated in the ($\bar{1}$10), (110), and (010) planes, respectively. The twofold symmetry
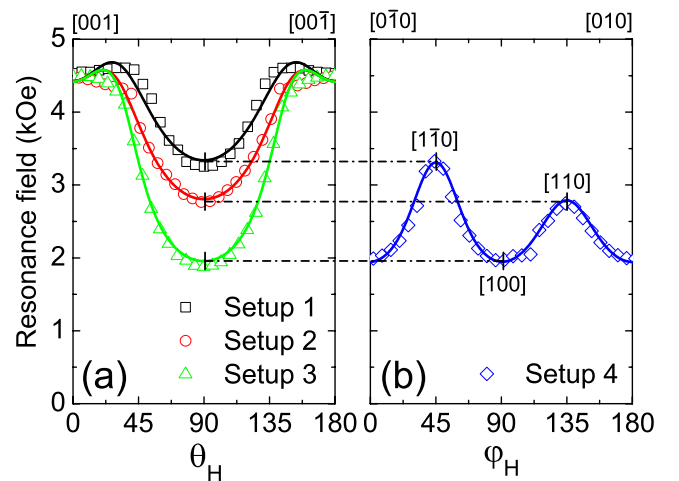
FIG. 4. (Color online) Angular dependence of the FMR field observed at 4 K for sample A grown on (001) plane, including all setups for that plane as shown in Fig. 1. Points are experimental; solid curves are theoretical fits.
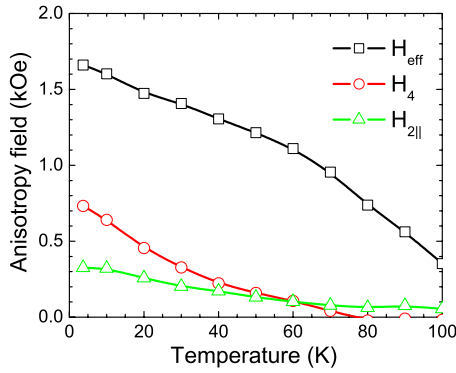
FIG. 5. (Color online) Temperature dependence of the cubic anisotropy field H_4 and uniaxial anisotropy fields H_{eff} and $H_{2\parallel}$ for sample A.

FIG. 6. (Color online) Selected FMR spectra for sample B taken at 4 K for θ_H from 0° to 180°, with **H** in the $(1\bar{1}2)$ plane (setup 5).

(rather than fourfold) about the 90° orientation for all three setups indicates that the angular dependence of FMR is dominated by the uniaxial anisotropy field. Note, however, the difference in the FMR position at 90° observed in setups 1 and 2, showing that **H** applied in the sample plane along the [110] and the $[1\bar{1}0]$ directions results in markedly different values of the FMR field.[8] The upward peaks in the curves near 25° and 155° in Fig. 4(a) result from the cubic anisotropy term. Figure 4(b) corresponds to setup 4, where **H** is confined to the sample plane. Note again that FMR occurs at different fields when **H** is parallel to [110] and to $[1\bar{1}0]$; and that the results in Fig. 4(b) are in excellent agreement with all in-plane FMR positions shown in Fig. 4(a), as indicated by the dash-dotted horizontal lines. Except for the difference between the resonance field for the [110] and $[1\bar{1}0]$ orientations, the angular dependence of FMR positions for the in-plane geometry is dominated by the cubic anisotropy term. One should also note that the resonance field has its lowest value when **H** is in the layer plane and aligned with the easy axis ([100] or [010]) in Figs. 4(a) and 4(b), exactly as is observed in FMR experiments on LT-MBE GaMnAs films grown on GaAs.[8,13]

The analysis of the angular dependence of the FMR data for sample A shown in Fig. 4 yields the following values of the anisotropy fields: $H_{eff}=(1,663\pm59)$ Oe; $H_{4\perp}=(858\pm72)$ Oe; $H_{4\parallel}=(770\pm65)$ Oe; and $H_{2\parallel}=(327\pm65)$ Oe. Note that $H_{4\perp}$ and $H_{4\parallel}$ differ by less than the margin of error. The angular dependence of FMR for sample A was also measured at a series of temperatures in increments of about 10 K apart for all four setups, allowing us to calculate anisotropy fields at each temperature. The results are plotted as a function of temperature in Fig. 5. Since the results for $H_{4\perp}$ and $H_{4\parallel}$ are within the margin of error at all temperatures, we conclude that the data obtained in this geometry are insufficient to meaningfully distinguish between the two cubic anisotropy fields and in Fig. 5 we therefore only plot their average value as H_4.

As seen in Fig. 5, the perpendicular effective uniaxial anisotropy field H_{eff} decreases rapidly from around 1660 to 300 Oe as the temperature increases from 4 to 100 K. The in-plane uniaxial and the cubic anisotropy fields have much smaller values compared to H_{eff}, indicating that the angular
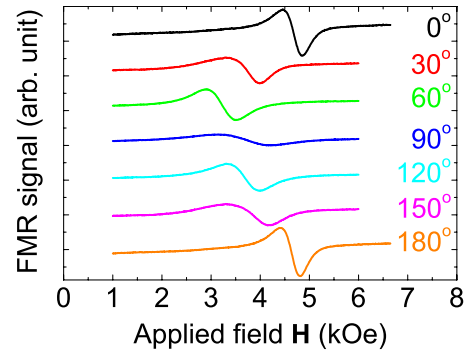
dependence of the FMR field is dominated by H_{eff} at all temperatures in these experiments. This behavior is similar to that observed on samples grown on higher-index planes discussed below and also to the behavior observed on $Ga_{1-x}Mn_xAs$ grown by LT-MBE.[13]

B. Results for II-PLM GaMnAs formed on the (110) plane

The angular dependence of FMR in II-PLM GaMnAs formed on the (110) plane (sample B) was studied in setups 5, 6, and 7. The FMR spectra observed at 4 K in setup 5 are shown in Fig. 6. Note that the FMR positions are asymmetric with respect to the 90° orientation in setup 5, consistent with the absence of fourfold symmetry in the $(1\bar{1}2)$ plane in which the field is rotated in this setup. An asymmetry in the FMR field is also observed in setup 6 (i.e., for field rotated in the $(1\bar{1}1)$ plane). In contrast, the spectra in setup 7 are twofold symmetric, as expected for the (110) plane geometry.

In Fig. 7 we plot the angular dependences of FMR observed at 4 K for sample B for all three setups. In the case of setup 5 (i.e., when **H** is rotated in the $(1\bar{1}2)$ plane), there is a
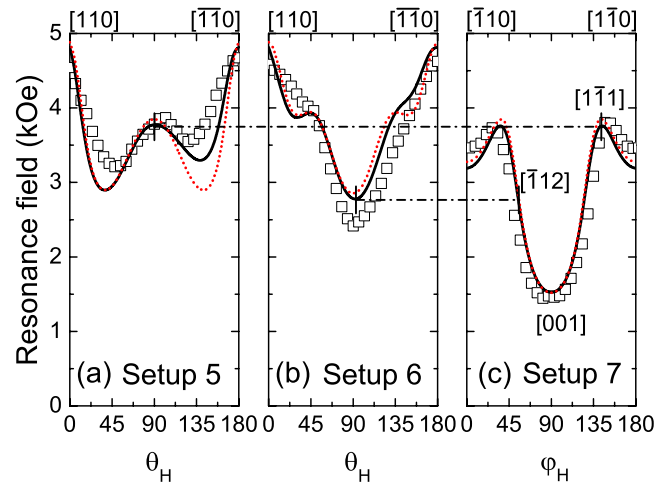

FIG. 7. (Color online) Angular dependence of FMR for sample B at 4.0 K observed in setup 5 (field rotated in the $(1\bar{1}2)$ plane), setup 6 (field rotated in the $(1\bar{1}1)$ plane), and setup 7 [field in the (110) plane]. Points are experimental; solid curves are best theoretical fits; dotted curves represent theoretical fits with $H_{4\perp}=H_{4\parallel}$.

large "dimple" in the angular dependence of the FMR field as the orientation of **H** approaches the in-plane $[1\bar{1}1]$ axis, with a pair of asymmetric valleys on the two sides of the dimple. The solid lines in the figure are theoretical fits obtained using Eq. (4). The agreement between theoretical fits and the experimental data is quite good, confirming the observed symmetries of the angular dependences of FMR in the three geometries.

The observed behavior can be understood in terms of contributions from the two cubic anisotropy fields $H_{4\perp}$ and $H_{4\parallel}$ defined along the $\langle 001 \rangle$ crystal axes, and the uniaxial anisotropy field H_{eff} normal to the sample plane. Theoretical fitting yields the value of the effective uniaxial anisotropy field as $H_{eff} \approx 1000$ Oe at 4 K. The in-plane cubic and the perpendicular cubic anisotropy fields $H_{4\perp}$ and $H_{4\parallel}$ are different for this sample: At 4 K, $H_{4\parallel} \approx 1400$ Oe, while $H_{4\perp} \approx 1000$ Oe. It is this difference between the two cubic anisotropy fields that is responsible for the asymmetry of the angular dependence of FMR observed in the two out-of-plane geometries, setups 5 and 6 in Fig. 7. To illustrate this point, we have also plotted (dotted curves) the theoretical angular dependence calculated with $H_{4\perp} = H_{4\parallel}$, which then shows complete symmetry around the in-plane 90° field orientation. The above results illustrate that, because the uniaxial and the cubic anisotropy fields are not coaxial for samples grown on the (110) plane, one is able to use this geometry to observe directly the difference between the two cubic anisotropies.

Finally, one should note that—similar to the case of A—the resonance field in sample B has its lowest value when **H** is in the layer plane and aligned with the easy axis in Fig. 7(c), setup 7 ([001], $\varphi_H = 90°$), as is observed in FMR experiments on LT-MBE GaMnAs films grown on GaAs. The resonance field observed in setups 5 and 6 in the in-plane orientation ($\theta_H = 90°$) is considerably above that field because in those cases **H** is not aligned with the easy axis when it reaches its in-plane ($\theta_H = 90°$) orientation.

C. Results for II-PLM GaMnAs samples grown on (311)A and (311)B surfaces

It is expected that the alloy composition, doping, layer thickness, and strain conditions can all lead to differences in the properties of an alloy. Additionally, the atomic arrangement of constituent elements corresponding to the orientation of the surface on which the layer is formed can also play a role in determining the physical properties of the resulting system. Recent combinatorial materials design methods[16,17] have predicted that the role of atomic configuration in $Ga_{1-x}Mn_xAs$—and especially the arrangement of the Mn ions—can have a dramatic effect on its magnetic properties.[18] Bearing this in mind, we have extended our FMR study also to $Ga_{1-x}Mn_xAs$ layers formed on higher-index planes—in this case, on (311) GaAs substrates.

As in the case of the (110) sample, we measured the FMR spectra on two $Ga_{1-x}Mn_xAs$ samples specimens implanted, respectively, on (311)A and (311)B surfaces of GaAs. We note parenthetically that (311)A and (311)B surfaces are polar, the former being As-rich and the latter Ga-rich, which
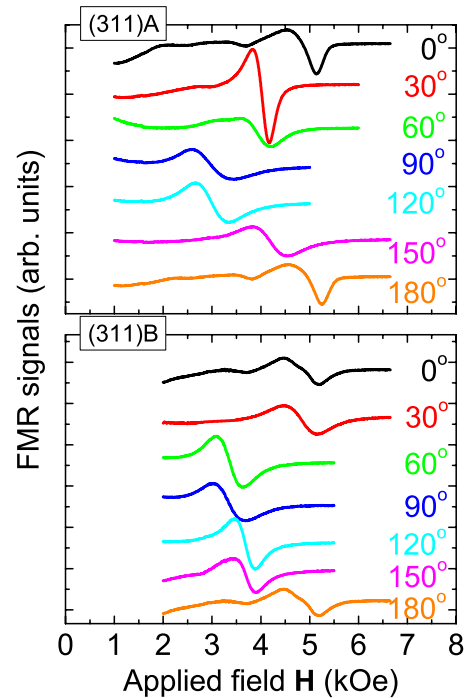

FIG. 8. (Color online) Selected FMR spectra for samples C and D taken at 4 K for θ_H from 0° to 180°, with **H** in the $(0\bar{1}1)$ plane (setup 8).

could in principle lead to different physical properties of the layers formed on surfaces so terminated. The FMR measurements were carried out as a function of θ_H and φ_H in setups 8, 9, and 10 shown in Fig. 1 for this layer orientation. Figure 8 shows the FMR spectra at 4 K for (311)A and (311)B samples obtained in setup 8, i.e., when **H** is rotated in the $(0\bar{1}1)$ plane. The spectra are asymmetric with respect to the $\theta_H = 90°$ orientation in setup 8 but are symmetric in setups 9 and 10, reflecting the respective symmetries of the planes in which the field is rotated. Traces of spin wave resonances are observed in both (311)A and (311)B samples below the FMR position in Fig. 8 at and near the perpendicular orientations, such as 0° and 180° in setups 8 and 9. These resonances are weaker than those seen typically in LT-MBE $Ga_{1-x}Mn_xAs$ layers,[8,13] possibly because the boundary between $Ga_{1-x}Mn_xAs$ and the GaAs substrate is less sharp in the II-PLM material.

The angular dependence of FMR for (311)A and (311)B specimens (samples C and D) was measured at 4, 25, and 50 K in setups 8, 9, and 10. In Fig. 9 we show the angular dependence for sample D observed at 4 K in these three setups. Theoretical fits obtained using Eq. (4), shown as solid curves in Fig. 9, are in very good agreement with experimental data. Note that the calculated results reflect closely the observed symmetry of the angular dependence of FMR in each plane. The fits to the data obtained on sample C corresponding to the layer formed on the (311)A plane show comparably good agreement. These fitting results show that the observed angular behavior of FMR can again be understood in terms of contributions from the cubic anisotropy field H_4 parallel to the $\langle 001 \rangle$ axes, and the uniaxial anisotropy field H_{eff} normal to the sample plane, i.e., in this case parallel to
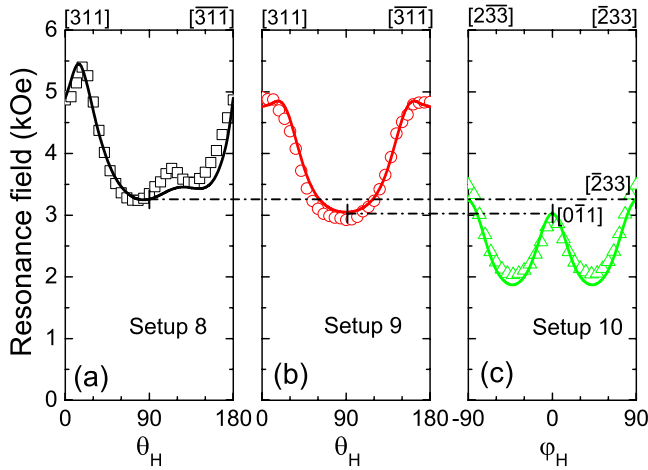
FIG. 9. (Color online) Angular dependence of FMR for sample D observed at 4 K in setups 8, 9, and 10. Points are experimental; solid curves are theoretical fits.
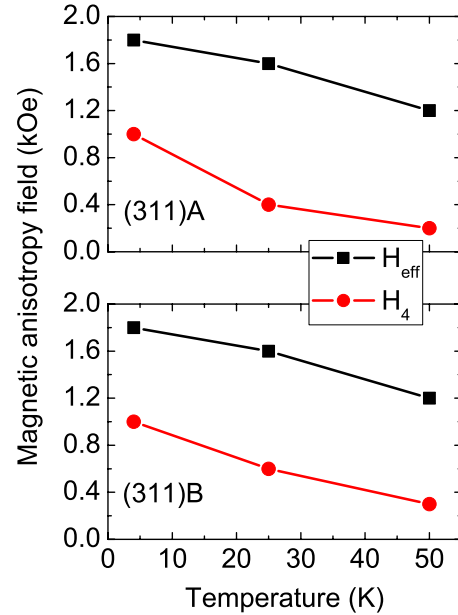

FIG. 10. (Color online) Temperature dependence of the cubic magnetic anisotropy field H_4 and the effective uniaxial magnetic anisotropy field H_{eff} for samples C and D.

the [311] direction.[12,14,19] Note that here, as in the case of the (110) sample, we do not distinguish between $H_{4\perp}$ and $H_{4\parallel}$; and we also no longer distinguish between anisotropy fields along the [110] and [1$\bar{1}$0] directions. Such (small) differences can only be identified in data obtained in sample A, which has the highest in-plane symmetry of the series of geometries examined in this study.

Note again the agreement between the FMR positions in Setups 8 and 9 when the field reaches the in-plane orientation ($\theta_H=90°$) and the FMR positions in the corresponding orientations observed in the in-plane scan in setup 10, as indicated by the dash-dotted lines. It is also gratifying that the value of FMR field for the [0$\bar{1}$1] orientation (maximum value in setup 10 and minimum in setup 9) is very close to the value of FMR observed for the in-plane [110] orientations for samples A and B [see Figs. 4(a), 4(b), and 7(c)]. This consistency is an indication that the magnetic properties of the samples formed by the II-PLM process—and, thus, the degree of Mn incorporation—are quite similar for the entire sample series used in these experiments.

The best fits shown in Fig. 9 yield the value of the cubic anisotropy field H_4 of ~1000 Oe at 4 K, and the effective uniaxial anisotropy field H_{eff} of ~1800 Oe at that temperature. The cubic anisotropy field H_4 obtained in our analysis is smaller than the value reported by Bihler *et al.*,[19] who studied (311)A Ga$_{1-x}$Mn$_x$As layers grown by LT-MBE. To estimate the behavior of the anisotropy parameters for samples C and D as a function of temperature, we have also measured and analyzed the angular dependence of FMR at 25 and 50 K for both samples. The results are shown in Fig. 10. Both magnetic anisotropy fields decrease with increasing temperature, the value of H_{eff} being always larger than H_4.

D. Summary of angular dependence of FMR field in II-PLM GaMnAs

Based on the results discussed in Sec. IV A–IV C, we conclude that the angular and temperature dependences of FMR positions observed in II-PLM Ga$_{1-x}$Mn$_x$As can be sat-

isfactorily represented by a magnetic-free-energy density defined in terms of cubic and uniaxial anisotropy terms, similar to the results obtained on LT-MBE Ga$_{1-x}$Mn$_x$As. Moreover, the observed values of the anisotropy fields obtained from the II-PLM Ga$_{1-x}$Mn$_x$As experiments are of the same order of magnitude as those from LT-MBE Ga$_{1-x}$Mn$_x$As. We can therefore conclude that the magnetic anisotropy is an intrinsic property in Ga$_{1-x}$Mn$_x$As system, which depends strongly on Mn and hole concentrations, but does not depend in any essential way on the method of synthesis. Furthermore, by comparing the results from II-PLM Ga$_{1-x}$Mn$_x$As synthesized on different crystal planes, i.e., on (100), (110), and (311) surfaces, we notice no signs indicating that there exists a specific relationship between the arrangement of Mn ions and the orientation of the surface. In particular, we observe excellent consistency between the FMR fields when the external field is applied along the same crystallographic directions in samples grown on the different crystal planes. We conclude from this that the Mn distribution in Ga$_{1-x}$Mn$_x$As is relatively random for all surface orientations, suggesting that it may be difficult to control the arrangement of Mn ions in Ga$_{1-x}$Mn$_x$As by choosing specific growth directions.

V. FMR LINE WIDTH

As was already noted, the second term in the Landau-Lifshitz-Gilbert equation—$\frac{\alpha}{(\gamma \cdot M_S)} \cdot \left[\mathbf{M} \times \frac{\partial \mathbf{M}}{\partial t} \right]$—provides information on the relaxation rate of the magnetization, which manifests itself as the peak-to-peak FMR linewidth ΔH_{pp}.[10,11] As part of this study we have also investigated ΔH_{pp} in II-PLM Ga$_{1-x}$Mn$_x$As samples as a function of field orientation and temperature. Although the mechanisms determining ΔH_{pp} are far from understood in Ga$_{1-x}$Mn$_x$As, it will be shown below that even a semiphenomenological analysis

of the linewidth provides valuable information about the existence of local fluctuations of magnetic properties within the material.

The resonance broadening ΔH_{pp} is usually caused by two mechanisms: an intrinsic (often called Gilbert) damping of the magnetization; and damping due to magnetic inhomogeneities in the ferromagnetic material. This can be expressed as follows:[11,20]

$$\Delta H_{pp} = \Delta H_{inhom} + \frac{2}{\sqrt{3}} \frac{G}{\gamma^2 M} \omega. \qquad (5)$$

Here the second term—the Gilbert damping—reflects "viscous" damping of the precessive motion of the magnetization associated with FMR, a process that is directly proportional to frequency, as seen in Eq. (5). The first term, on the other hand—the inhomogeneous broadening ΔH_{inhom}—is caused by sample imperfections, and can be viewed as arising from a distribution of local resonance fields. The imperfections causing such broadening of FMR may include local fluctuations of alloy composition and hole concentration, as well as local fluctuations in the orientation of magnetic anisotropy fields. As a consequence, this term is expected to depend on the orientation of the applied magnetic field. This part of the FMR linewidth thus provides a measure of the magnetic homogeneity of the sample. The overall linewidth can be approximated by:[7]

$$\Delta H_{pp} = \Delta H_0 + \Delta \theta \frac{\delta H_r}{\delta \theta_H} + \Delta \varphi \frac{\delta H_r}{\delta \varphi_H} + \Delta H_{int} \frac{\delta H_r}{\delta H_{int}}, \qquad (6)$$

where ΔH_0 contains the Gilbert damping term lumped together with angle-independent contributions from randomly distributed defects, and H_r denotes the value of the FMR field at a given orientation. The second and third terms on the right are due to small local variations ($\Delta \theta$ and $\Delta \varphi$) of the anisotropy axes and are therefore expected to depend on the angle of the applied field. The fourth term in Eq. (6) is due to a distribution ΔH_{int} of the magnitude of the internal field H_{int}. Note that H_{int} reduces equal to the effective anisotropy field $H_{eff} = 4\pi M - H_{2\perp}$ when cubic anisotropy terms are small.

We have measured the FMR linewidth as a function of applied field orientation for each setup shown in Fig. 1. The points in Fig. 11 show the angular dependence of ΔH_{pp} observed at 4.0 K for sample A [i.e., the sample formed on the (001) plane] for the four setups corresponding to this sample geometry. The observed data were analyzed by fitting with Eq. (6). The fitting results are in reasonable agreement with the experimental results, indicating that the FMR linewidth of this sample is dominated by inhomogeneous broadening. Quantitatively the observed angular dependence of ΔH_{pp} is primarily determined by the terms $\Delta \theta \frac{\delta H_r}{\delta \theta_H}$ and $\Delta \varphi \frac{\delta H_r}{\delta \varphi_H}$. Best fits (shown by continuous curves in Fig. 11), obtained when these terms are dominant and the remaining terms in Eq. (6) are negligible in comparison, yield $\Delta \theta$ and $\Delta \varphi$ of about 6°.

The angular dependence of ΔH_{pp} in II-PLM $Ga_{1-x}Mn_xAs$ is similar to that observed in annealed $Ga_{1-x}Mn_xAs$ samples grown by LT-MBE,[8] indicating that the inhomogeneous broadening in both II-PLM and annealed LT-MBE
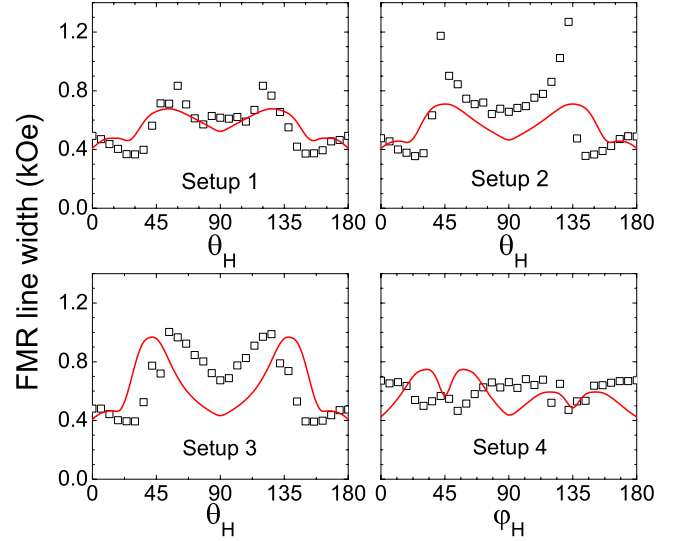

FIG. 11. (Color online) Angular dependence of FMR linewidth for sample A at 4.0 K observed in four setups corresponding to the (001) plane geometry of this sample. Points are experimental; continuous curves are best theoretical fits for each setup obtained using Eq. (6).

$Ga_{1-x}Mn_xAs$ samples results from crystal imperfections such as vacancies and/or other defects. However, the magnitude of ΔH_{pp} in the II-PLM $Ga_{1-x}Mn_xAs$ samples is considerably larger ($\Delta H_{pp} > 400$ Oe), suggesting that there exists a larger concentration of such imperfections in the II-PLM material.

In principle, one should be able to use a similar method as that just described to analyze the linewidth in samples fabricated on other surface orientations. However, we find that the angular dependences of ΔH_{pp} observed in samples B, C, and D are much more complicated than those observed in sample A and for those samples we were unable to obtain fits comparable to those shown in Fig. 11 using Eq. (6). We will therefore restrict ourselves only to a qualitative discussion of the linewidth in samples grown on higher-index planes. We should note, however, that the correspondence in symmetry between the angular dependences of the linewidth and the FMR position (and thus of its angular derivatives) is also quite evident in the case of those higher-index-plane samples, suggesting that the linewidth in these samples is again dominated by inhomogeneous broadening.

The angular dependence of the FMR linewidth ΔH_{pp} for sample D grown on the (311)B plane is shown in Fig. 12 for the three setups corresponding to the geometry of this sample. The linewidth has a strong angular variation at 4 K, which gradually becomes weaker with increasing temperature. It is obvious that the angular dependence of the FMR linewidth in setup 8 is asymmetric about the 90° orientation while those in setups 9 and 10 are symmetric about 90° and 0°, respectively, similar to the angular dependence of the FMR position seen in Fig. 9. In setup 8 the FMR linewidth is very large at approximately the field orientation corresponding to the prominent dimple in Fig. 9 (near 110°). It is rather striking that the linewidth shows sharp peaks at several well-defined orientations ($[311]$, $[\bar{2}33]$, and $[0\bar{1}1]$) and at some intermediate angles (36° and 144° in setups 8 and 9). We find
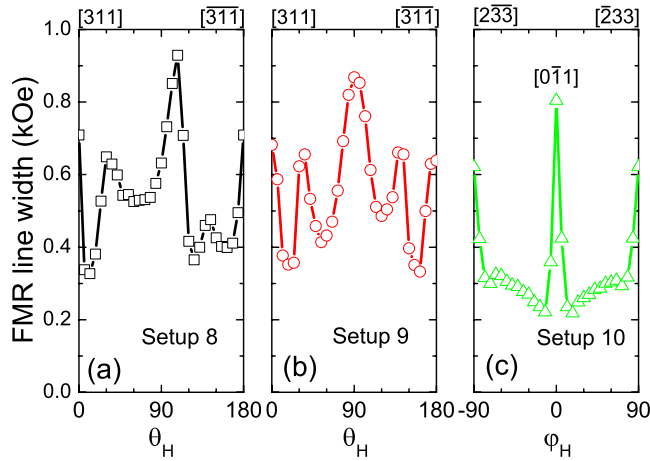
FIG. 12. (Color online) Angular dependence of FMR line width at 4.0 K for sample D observed in setups 8 to 10. Points are experimental; solid curves are guides for the eye.

that the peaks in the intermediate angles can be explained by Eq. (6), but the peaks in specific orientations and at the dimple position are not understood. Therefore, although we see a clear relationship between the respective symmetries of the angular behavior of the FMR position and the linewidth, the mechanism of linewidth in $Ga_{1-x}Mn_xAs$ fabricated on high-index substrate definitely requires further investigation.

VI. CONCLUDING REMARKS

We have studied the angular and temperature dependences of FMR in $Ga_{1-x}Mn_xAs$ samples fabricated by Mn ion implantation and pulsed laser melting on (001), (110), (311)A, and (311)B GaAs surfaces. The angular dependence of the FMR position was analyzed using the Stoner-Wohlfarth model and LLG equation in order to obtain the values of magnetic anisotropy parameters for this material. For the

sample grown on the (001) plane (sample A) the angular dependence of the FMR field observed in out-of-plane geometries was found to be dominated by uniaxial anisotropy in out-of-plane geometries; but in the in-plane geometry (corresponding to setup 4 in Fig. 1) cubic anisotropy was found to be dominant at low temperatures. For the (110) or (311) samples the observed angular behavior of FMR can, similarly, be described in terms of contributions from cubic anisotropy fields H_4 parallel to the $\langle 001 \rangle$ axes and an effective uniaxial anisotropy field H_{eff} normal to the plane of the film (i.e., along the [110] and [$\bar{3}$11] directions, respectively). The property of the sample formed on the (311)A surface is very similar to that of grown on (311)B, the effective uniaxial anisotropy field being much larger than the cubic anisotropy field.

We have also investigated the angular dependence of FMR linewidth ΔH_{pp} in these samples, and found that in the sample grown on the (001) crystal plane (sample A) the value of ΔH_{pp} is primarily determined by the derivative of the angular dependence of the FMR field, suggesting that the linewidth in II-PLM $Ga_{1-x}Mn_xAs$ results primarily from inhomogeneous broadening due to local fluctuations of magnetic properties, such as small local variations of the anisotropy fields. Our results show that magnetic anisotropy in II-PLM $Ga_{1-x}Mn_xAs$, as well as the behavior of its linewidth, are fundamentally similar to those seen in $Ga_{1-x}Mn_xAs$ samples grown by LT-MBE, indicating that materials formed by these two very different growth methods have very similar magnetic properties.

*xliu2@nd.edu

†furdyna.1@nd.edu

[1] A. H. MacDonald, P. Schiffer, and N. Samarth, Nature Mater. **4**, 195 (2005).

[2] I. Žutić, J. Fabian, and S. Das Sarma, Rev. Mod. Phys. **76**, 323 (2004).

[3] H. Ohno, Science **281**, 951 (1998).

[4] M. A. Scarpulla, O. D. Dubon, K. M. Yu, O. Monteiro, M. R. Pillai, M. J. Aziz, and M. C. Ridgway, Appl. Phys. Lett. **82**, 1251 (2003).

[5] M. A. Scarpulla, B. L. Cardozo, R. Farshchi, W. M. Hlaing Oo, M. D. McCluskey, K. M. Yu, and O. D. Dubon, Phys. Rev. Lett. **95**, 207204 (2005).

[6] M. A. Scarpulla, R. Farshchi, P. R. Stone, R. V. Chopdekar, K. M. Yu, Y. Suzuki, and O. D. Dubon, J. Appl. Phys. **103**, 073913 (2008).

[7] M. Farle, Rep. Prog. Phys. **61**, 755 (1998).

[8] X. Liu and J. K. Furdyna, J. Phys.: Condens. Matter **19**, 165205 (2007).

[9] M. J. Aziz and C. W. White, Phys. Rev. Lett. **57**, 2675 (1986).

[10] A. Aspelmeier, M. Tischer, M. Farle, M. Russo, K. Baberschke, and D. Arvanitis, J. Magn. Magn. Mater. **146**, 256 (1995).

[11] *Ultrathin Magnetic Structures*, edited by B. Heinrich and J. A. C. Bland (Springer, Berlin, 1994).

[12] Y. Y. Zhou, X. Liu, J. K. Furdyna, M. A. Scarpulla, and O. D. Dubon, J. Supercond. Novel Magn. (to be published).

[13] X. Liu, Y. Sasaki, and J. K. Furdyna, Phys. Rev. B **67**, 205204 (2003).

[14] Y.-Y. Zhou, Ph. D. thesis, University of Notre Dame, 2008.

[15] U. Welp, V. K. Vlasko-Vlasov, X. Liu, J. K. Furdyna, and T. Wojtowicz, Phys. Rev. Lett. **90**, 167206 (2003).

[16] *Computer-Aided Molecular Design: Theory and Practice*, edited by L. E. K. Achenie, R. Gani, and V. Venkatsubramanian (Elsevier, Amsterdam, 2003).

[17] A. Franceschetti and A. Zunger, Nature (London) **402**, 60 (1999).

[18] A. Franceschetti, S. V. Dudiy, S. V. Barabash, A. Zunger, J. Xu, and M. van Schilfgaarde, Phys. Rev. Lett. **97**, 047202 (2006).

[19] C. Bihler, H. Huebl, M. S. Brandt, S. T. B. Goennenwein, M. Reinwald, U. Wurstbauer, M. Döppe, D. Weiss, and W. Wegscheider, Appl. Phys. Lett. **89**, 012507 (2006).

[20] W. Platow, A. N. Anisimov, G. L. Dunifer, M. Farle, and K. Baberschke, Phys. Rev. B **58**, 5611 (1998).